

Exergy Analysis and Modeling of Pilot-Scale Pyrolysis for Magnesium Oxide Preparation from Salt Lake Bischofite Industrial Waste

Hanlu Xu,[†] Hui Dong,* Liang Zhao, and Daokuan Cheng[†]Cite This: *ACS Omega* 2023, 8, 47153–47162

Read Online

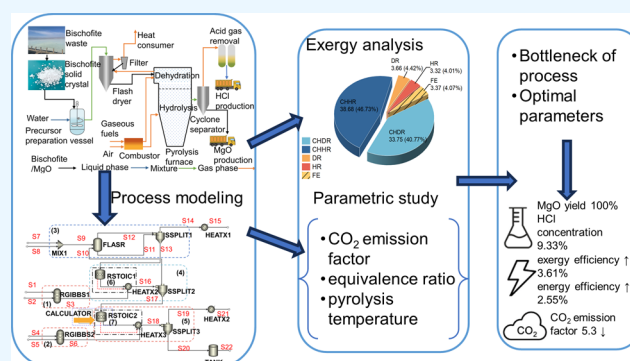
ACCESS |

Metrics & More

Article Recommendations

Supporting Information

ABSTRACT: Currently, the traditional magnesium oxide production process is facing exceptional challenges arising from carbon emission restrictions and environmental protection. Waste bischofite pyrolysis has attracted much attention as a promising technology to address these challenges. Nonetheless, this process has primarily been demonstrated on a laboratory scale, with limited studies on an industrial scale. A comprehensive exergy analysis was conducted for the entire process and individual subunits within the pyrolysis process to identify potential areas for process enhancement. A FORTRAN subroutine based on empirical correlations of pyrolysis product yields was developed considering the impact of decomposition reactions on the simulation. Furthermore, the optimization of energy and exergy efficiency of the system was discussed in terms of the carbon dioxide emission factor, equivalence ratio, and pyrolysis temperature. The results show that the primary energy bottleneck lies in the combustion phase. In addition, the optimal energy and exergy efficiency conditions are a carbon dioxide emission factor of 5.3, an equivalent ratio of 1.15, and a pyrolysis temperature of 1100 °C. In comparison to the pilot-scale conditions, the energy efficiency and exergy efficiency increase by 2.55 and 3.61%, respectively. At this time, the MgO yield is 100%, and the HCl concentration is above 9.33%.



1. INTRODUCTION

Due to rapid urbanization and industrialization in developing countries, magnesium (MgO) remains in high demand globally for applications in the iron and steel industry, cement manufacturing, and nonferrous metallurgy.^{1,2} According to data from the United States Geological Survey (USGS), China is responsible for 90.00% of the global production of magnesium refractories.³ The main raw material for manufacturing magnesium refractories is magnesite, which accounts for 76.90% of the overall output.⁴ The production of magnesium refractories from magnesite results in the release of carbon dioxide from the combustion of fuels and the decomposition of magnesite.¹ Consequently, China, the global leader in the magnesium metallurgical market, must assume the environmental responsibilities associated with magnesium mining, manufacturing, and smelting. Especially, the exploitation of magnesite has been restricted due to carbon emission control and environmental protection measures.⁵ Therefore, there is a need for new ways to extract magnesium resources due to the introduction of strict environmental legislation and growing concerns about greenhouse gas emissions and climate change.

Within the salt lake industry, potassium chloride (KCl) extraction generates industrial byproducts in evaporation ponds, including bischofite.^{6,7} Generally, bischofite ($\text{MgCl}_2 \cdot 6\text{H}_2\text{O}$) is a

magnesium chloride mineral with crystallization water.⁸ However, the accumulation of large quantities of bischofite waste threatens the sustainable development and ecological environment of the salt lake industry.^{5,9} Unfortunately, the utilization rate of bischofite remains low, with less than 1% of the total waste being effectively utilized.⁴ Statistical data from 2019 in China indicate that the production of potassium chloride was 804,000 tons, while solid waste bischofite exceeded an annual volume of 80 million tons.¹⁰ In recent years, bischofite has shown the potential to produce magnesium materials higher in quality than magnesite, making it a promising and sustainable alternative resource.

Researchers have recently developed techniques for converting bischofite to MgO by adding alkaline precipitants, such as lime milk precipitation, sodium-base precipitation, and ammonia precipitation.^{11–14} Among the various alkaline-based precipitation methods, such as lime milk or ammonia

Received: September 18, 2023

Revised: November 9, 2023

Accepted: November 13, 2023

Published: November 28, 2023



precipitation, it has been demonstrated that they exhibit the highest feasibility in treating bischofite wastes. Consequently, a majority of pilot plants use lime milk or ammonia precipitation systems. However, the commercial application of these methods still needs to be improved due to their drawbacks. For example, impurities in the precipitant and suboptimal filtration efficiency can adversely impact the treatment process, increasing the operating costs. Additionally, the precipitate magnesium-containing solids require further calcination to produce MgO, thereby introducing complexity into the production process.

To overcome the drawbacks of alkaline-based precipitation techniques, high-temperature pyrolysis of bischofite has emerged as the most promising MgO conversion technology that may create reduced expenses in the near future. In the early 1960s, Dr. J. Aman from the Hebrew University began investigating the “Aman process,” using pyrolysis technology to convert bischofite into high-purity MgO.^{15,16} The pyrolysis technology was pushed into the initial pilot phase by Dead Sea Periclase Ltd. in Israel in the 1980s, with the increase in KCl production.¹⁷ When the bischofite waste is exposed to pyrohydrolysis/spray roasting at temperatures between 800 and 1000 °C, it yields MgO particles, HCl gas, and H₂O vapor.¹⁸ This method offers many benefits over other techniques such as reduced contamination of the final product and simplified production and operation. In this sense, the substantial potential of bischofite pyrolysis has ignited interest in its large-scale industrial production.

Despite the promising potential benefits of bischofite pyrolysis, there are several challenges that hinder its commercialization, for example, high energy consumption, incomplete product decomposition, and equipment corrosion.^{18,19} However, current studies have focused on the pyrolysis mechanism, product value addition, and pyrolysis furnace design to overcome these challenges. Li et al.⁸ used thermogravimetry and X-ray diffraction to investigate the bischofite pyrolysis mechanism and products at different temperatures, heating rates, and ambient atmospheres. The findings showed that MgO, a stable product, was formed at a calcination temperature of 700 °C. Additionally, ultrasonic washing and secondary calcination might further improve the purity of MgO. Zhang et al.¹⁸ investigated the feasibility of the bischofite to MgO using a radio frequency induction thermal plasma process. Their results demonstrated the capability of this process to yield two high-purity MgO structures: spherical MgO nanoparticles with dimensions of 20–40 nm and one-dimensional MgO nanoribbons measuring 100 nm. Du et al.²⁰ designed and investigated a spray pyrolysis furnace to produce MgO from bischofite using computational fluid dynamics. Their study facilitated the acquisition of temperature and species distribution data within the continuous phase and the separation efficiency (%) and residence time (s) of the dispersed particles.

Despite the numerous laboratory studies, the commercialization of the bischofite pyrolysis process still requires a while due to the lack of engineering scaled-up data. Currently, a typical thermodynamic equilibrium study was conducted by Bakker et al.²¹ The key node parameters of the process were determined based on the thermal decomposition mechanism obtained from thermogravimetric experiments and X-ray diffraction (XRD) characterization. Meanwhile, the molar fractions of gaseous products, including CO₂, HCl, and H₂O, were estimated. The pyrolysis furnace temperature and the rate of decomposition reactions can influence the production of gaseous products. Consequently, the thermodynamic equilibrium model em-

ployed by Bakker et al.²¹ would lead to overestimating CO₂, HCl, and H₂O yields. In addition, Luong et al.²² assessed CO₂ emissions resulting from the bischofite pyrolysis process, considering the theoretical reaction enthalpy (kJ/mol) and the thermal efficiency (%). Compared with other alternative process routes for MgO production, the bischofite pyrolysis process has the lowest environmental burden. However, previous studies had focused only on the conceptual designs of energy assessment and environmental impacts of the bischofite pyrolysis process, overlooking an analysis of the quantities and variations in the energy of the process components or devices along with incorporating experimental data into process simulation software. As a result, previous findings face challenges in providing engineering guidance on production energy consumption and improvements at the level of individual process plants.

Comprehension of energy consumption throughout the entire process is of paramount importance. Exergy analysis is a powerful energy analysis tool, reflecting the potential loss of work due to the irreversibility of the second law of thermodynamics. It facilitates the identification and quantification of exergy destruction, enabling the calculation of the exergy efficiency. It is understood that there is a lack of information about the design, construction, and operation of facilities for large-scale production of the bischofite pyrolysis process. To this end, modeling and exergy analysis with the help of the Aspen Plus tool has proven beneficial in assessing the energy efficiency ($\eta\%$) and exergy efficiency ($\varepsilon\%$) of engineering processes. This tool has been widely used in studies of other industrial systems, such as the process of synthesizing monochloromethane by methanol hydrochlorination, where the energy loss (MW), exergy destruction (MW), and exergy efficiency ($\varepsilon\%$) of the process components were analyzed. The findings revealed that the reactor, followed by the absorber, had the maximum exergy destruction.²³ In another study, Mohamadi-Baghmolaei et al.²⁴ developed a simulation platform and thermodynamic modeling methodology for a sour gas recovery plant. The analysis showed that the stripper and absorber towers were key pieces of equipment with significant potential for improvement, offering the prospect of mitigating substantial carbon dioxide emissions. In addition, Aspen Plus modeling can also replicate precise unit activities and reliably estimate the physical properties and connections of pure substances and complex mixtures. Thus, Aspen Plus modeling and exergy analysis also serve as the first step in evaluating emerging processes under sustainability criteria.^{25,26} For example, Chen et al.²⁷ proposed a novel concentrating solar power plant using calcium ring-based thermochemical energy storage to eliminate the dependence of power generation on the carbonization reaction in sunlight. The results showed a global storage exergy efficiency ($\varepsilon\%$) of over 37% and a global power efficiency of about 48%, comparable to those of state-of-the-art systems. Liu et al.²⁸ suggested a waste heat-driven system coupled with electricity and refrigeration. An improvement strategy combining the self-improvement of components, improvement of other components, and system optimization was proposed using exergy analysis and advanced exergy analysis. However, there is no relevant literature on the simulation prediction of the process of MgO preparation by bischofite pyrolysis. Simulation modeling and analysis of the pyrolysis process are crucial for large-scale industrial production as they allow decision-makers to enhance and assess the sustainability criteria of the process.

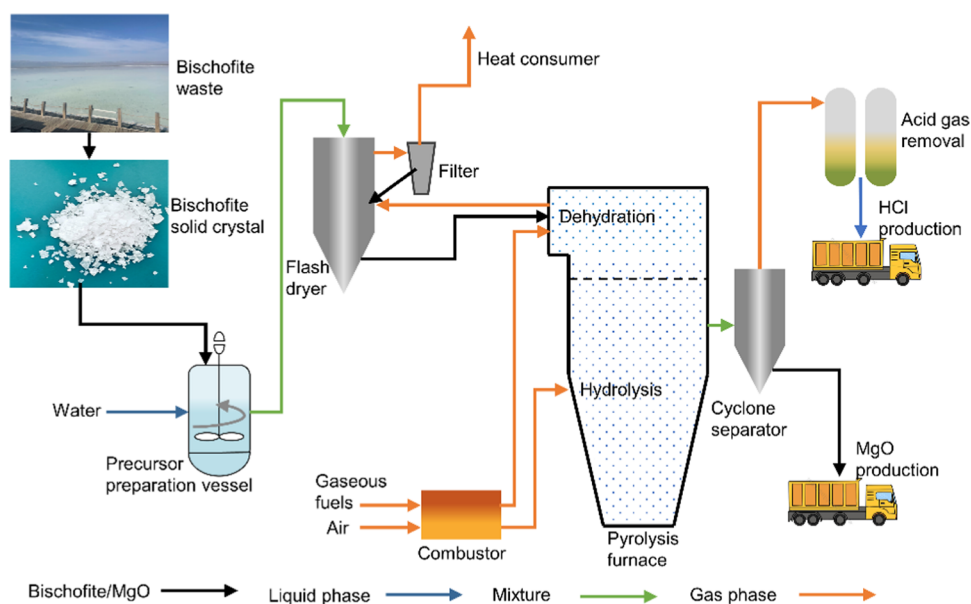


Figure 1. Schematic of the bischofite pyrolysis process.

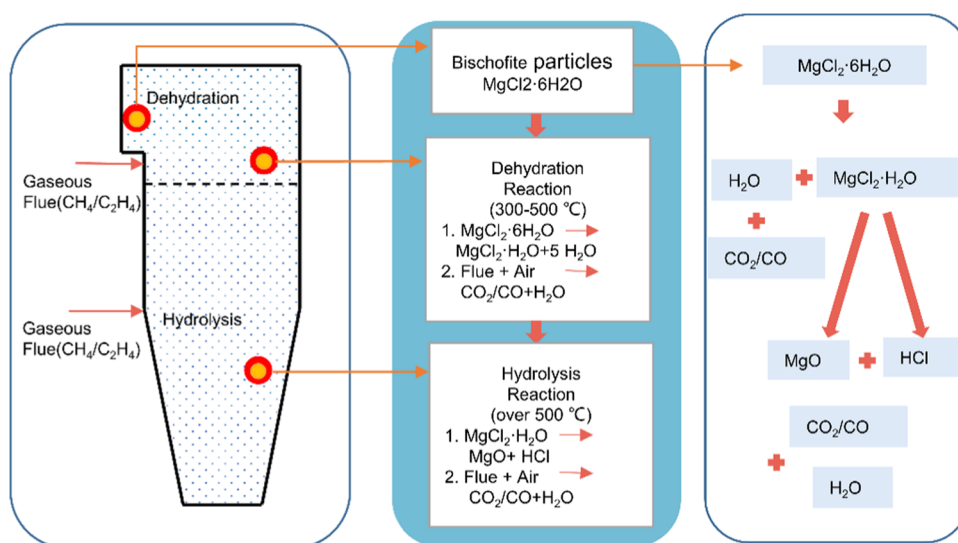


Figure 2. Continuous reaction mechanism in the pyrolysis furnace.

This work aims to enhance energy efficiency ($\eta\%$) and minimize exergy destruction (MW), considering the quality of MgO production and HCl concentration in the example of the Liaoning Dongda Powder pilot-scale system plant. The principal contribution is the simulation of the bischofite pyrolysis process by implementing the Aspen Plus simulator. A comprehensive assessment of the quantitative alterations in the energy of the pyrolysis process unit components was performed by exergy analysis. Meanwhile, the primary areas with potential for enhancement were identified. In addition, the energy efficiency ($\eta\%$) and exergy efficiency ($\varepsilon\%$) of the system were optimized in terms of the carbon dioxide emission factor, equivalence ratio, and pyrolysis temperature to fulfill the requirements of both MgO yield and HCl concentration. Considering the influence of the decomposition reaction on the simulation accuracy, the Aspen Plus model was developed in combination with the FORTRAN subroutine based on the empirical correlation of the experimentally obtained pyrolysis product yields. This work will provide an effective way for the large-scale production of

bischofite pyrolysis technology to improve the energy efficiency of the whole thermal system.

2. SYSTEM MODELING AND ANALYSIS

2.1. Bischofite Pyrolysis Process Description.

This investigation measured the exergy destruction (MW) and exergy efficiency ($\varepsilon\%$) of a pilot-scale bischofite pyrolysis unit at the Dongda Powder Plant in Liaoning Province, China. According to the laboratory data from the authors, the plant was able to capture around 30,000 tons of MgO per year, with a bischofite flow rate of 4.83 kg/s. The raw materials for the plant were sourced from Qinghai Western Magnesium Co., Ltd., and bischofite accounted for 86.5% of the composition.²⁹

Figure 1 depicts a typical schematic of the bischofite pyrolysis pilot-scale process. Generally, bischofite is a large solid crystal formed in evaporation ponds. If bischofite is fed directly into the pyrolysis furnace, it is not conducive to pyrolysis, heat transfer, and mass transfer. Therefore, a saturated precursor solution is prepared by mixing bischofite with liquid water, taking

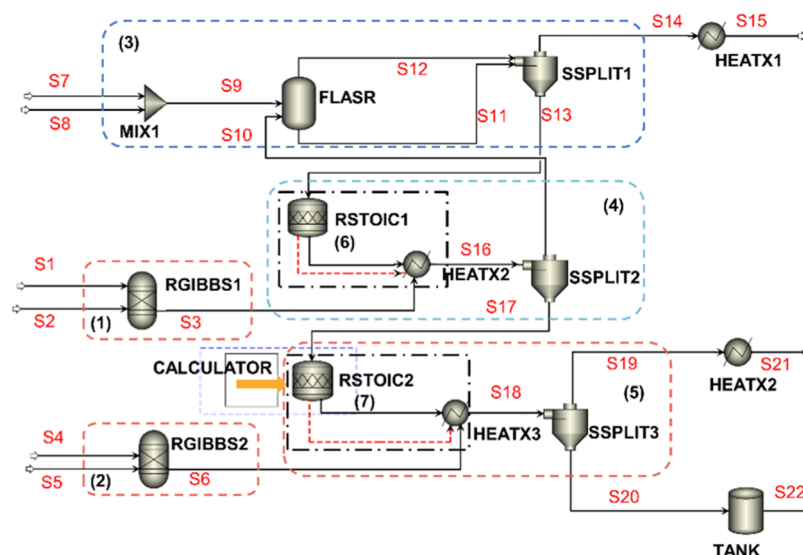


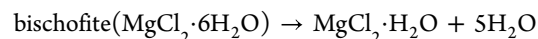
Figure 3. Aspen Plus flowsheet for the bischofite pyrolysis system: (1) combustion heating-hydrolysis reaction; (2) combustion heating-dehydration reaction; (3) flash evaporation; (4) dehydration reaction; (5) hydrolysis reaction; (6) dehydration module; (7) hydrolysis module; S1–S22 material stream.

advantage of the water-soluble nature of bischofite. First, the prepared saturated precursor solution is delivered into a flash dryer, where the water in the saturated precursor solution is evaporated, leaving uniformly sized solid particles. The heated flue gases produced during pyrolysis provided the heat for the flash drying unit. A filter removes fine bischofite particles from the flue gas exiting the flash dryer. Therefore, the saturated precursor evaporation system raises the temperature of bischofite entering the furnace and homogenizes the particles. Then, dried bischofite enters the pyrolysis furnace as a raw material and undergoes dehydration and hydrolysis. Graded combustion of gaseous fuels maintains an even temperature in the pyrolysis furnace for dehydration and hydrolysis. Finally, a cyclone separator separates the MgO particles produced during bischofite pyrolysis from the fuel gas. In addition, hydrochloric acid may also be made using the HCl gas produced during pyrolysis. Detailed information on the operating conditions and the composition of the fuel gas are provided in Table S1 (Supporting Information).

2.2. Process Simulation. The bischofite pyrolysis furnace plays a crucial role in the entire system, as several processes occur consecutively within the furnace, including dehydration and hydrolysis reactions. To simulate bischofite pyrolysis, a sequential modular modeling technique has been proposed, which has already been applied to simulate biomass pyrolysis gasifiers.^{26,30} The technique involves dividing the pyrolysis furnace system into dehydration and hydrolysis modules, enabling simulation convergence. In this section, Aspen Plus V11 software is used to model the bischofite pyrolysis pilot-scale process by describing the reaction mechanism within the furnace and modeling it using the Aspen Plus simulator.

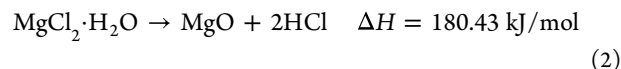
2.2.1. Dehydration Reaction. Figure 2 depicts the dehydration and hydrolysis reactions that occur while bischofite passes through the pyrolysis reactor. At temperatures ranging from 300 to 500 °C, bischofite is transformed into H₂O vapor and solid MgCl₂·H₂O.^{31,32} The required heat for this reaction is produced by hot flue gases that are generated from the combustion of gaseous fuels and can reach temperatures between 800 and 1000 °C. As a result, the dehydration reaction occurs immediately at the top of the pyrolysis reactor. Published

studies²⁹ by our team have shown that the dehydration reaction involves at least three subreactions. We estimated the reaction enthalpies and formulated the total dehydration equation to simplify the system modeling.



$$\Delta H = 322.81 \text{ kJ/mol} \quad (1)$$

2.2.2. Hydrolysis Reaction. Subsequently, the MgCl₂·H₂O solid particles fall to the bottom of the pyrolysis reactor. Similarly, the energy for the hydrolysis reaction is supplied through the combustion of gaseous fuel. At temperatures over 500 °C, MgCl₂·H₂O undergoes further pyrolysis, yielding the pyrolysis gases H₂O and HCl and the solid product MgO. In addition, the pyrolysis gases also include CO₂, CO, and H₂O produced by fuel combustion. The following equation represents the hydrolysis reaction



Bischofite pyrolysis is a highly complicated phenomenon characterized by numerous physicochemical transformations and the formation of intermediate products.^{31,33} However, we are concerned about the ultimate production of MgO and HCl in engineering. Therefore, only the conversion reaction of MgCl₂·H₂O to MgO is focused. Based on thermogravimetric analysis (TGA), we obtained the product yield in the range of 500–800 °C. Empirical equations relating temperature to the yields of Y_{MgCl₂·H₂O}, Y_{MgO}, and Y_{HCl} were fitted to the bischofite hydrolysis reaction by drawing on Trninić et al.³⁴ The results were obtained as follows

$$Y_{\text{MgCl}_2 \cdot \text{H}_2\text{O}} = (-4.48 \times 10^{-5}) \times T^2 + 0.058 \times T - 17.91 \quad (3)$$

$$Y_{\text{MgO}} = (1.59 \times 10^{-5}) \times T^2 - 0.021 \times T + 6.69 \quad (4)$$

$$Y_{\text{HCl}} = (2.89 \times 10^{-5}) \times T^2 - 0.037 \times T + 12.22 \quad (5)$$

2.3. Aspen Plus Modeling. This section describes the establishment of a simulation platform using Aspen Plus software, which considers the actual operating conditions. The Aspen Plus simulation mainly comprises identifying the chemical composition, establishing the thermodynamic equations, selecting the appropriate operating units, and configuring the input specifications.²⁶ The simulations employed the Peng–Robinson–Boston Mathias method, extensively used for pyrolysis and hydrocarbon fuel combustion.³⁰ Since the pyrolysis furnace contains solid and gas phases, MCINCPD depicts streams, including the solid MgO and the gas-phase mixture.

Figure 3 depicts the Aspen Plus flowsheet for the bischofite pyrolysis system. First, bischofite waste S7 and water S8 are mixed into a saturated liquid in a mixer (MIX1). The heat transported by decomposition gases S10 is used as a heat source in the flash dryer (FLASR) to dry saturated liquids S9. The produced dry particles S13 are separated from water vapor S14 using a separator (SSPLIT1). In this situation, separated water vapor S14 can offer the heat consumer, which is sent into the heater (HEATX1) and cooled to ambient temperature to compute the available sensible heat. Then, dried bischofite S3 is fed to the pyrolyzer reactor. Considering the chemical events inside the pyrolysis furnace, the pyrolysis furnace can be divided into a (6) dehydration module and (7) hydrolysis module. The dehydration module contains decomposition and heat transfer units, of which the decomposition unit utilizes a dehydration reactor (RSTOIC1) to convert the bischofite to $\text{MgCl}_2 \cdot \text{H}_2\text{O}$ and H_2O with 100% conversion. The heat exchange unit (HEATX2) performs heat exchange between decomposition products S16 and hot flue gases S3 generated by combustion. Following the heat exchange, flue gas S3 and decomposition product S16 are separated in a cyclone separator (SSPLIT2). Like dehydration, hydrolysis comprises a reaction module (RSTOIC2) and a heat transfer (HEATX3) module. To further analyze the $\text{MgCl}_2 \cdot \text{H}_2\text{O}$ decomposition as a function of pyrolysis temperature, eqs 3–5 are integrated into the internal FORTRAN subroutine of the calculator module. The pyrolysis temperature refers to the temperature that leaves the heat transfer module. Finally, the MgO solid product S19 and decomposition gas S20 are sent through a cyclone separator (SSPLIT3). The decomposition flue gas and solid product MgO are directed to the HEATX2 and TANK model and cooled to ambient temperature to determine heat loss. The dehydration and hydrolysis processes are heated in a gas-fuel combustion reactor (RGIBBS1,2). In addition, the simulation results were verified by using the operational data collected from the pilot experiment. The simulation phase is defined by the concentrations of HCl, CO_2 , N_2 , and H_2O in the pyrolysis gas, as well as the dehydration and hydrolysis temperatures. The operational and simulation data are reported in Table 1.

Table 1. Comparison of the Operation and Simulation Data[†]

parameter	operation	simulation	error %
HCl outlet concentration (mol %)	6.85	6.88	0.43
CO_2 outlet concentration (mol %)	8.14	8.48	4.18
N_2 outlet concentration (mol %)	66.00	66.90	1.36
H_2O outlet concentration (mol %)	16.30	17.00	4.29
dehydration temperature (K)	858.8	869.6	1.26
hydrolysis temperature (K)	1090.3	1075.4	1.36

[†]Error% = $|x_{\text{op}} - x_{\text{sim}}| / x_{\text{op}} \times 100\%$

2.4. Exergy Analysis. A comprehensive analysis of the bischofite pyrolysis energy consumption is essential for the commercial-scale process. Exergy analysis provides a practical tool for exploring the system irreversibility.³⁵ Irreversibility is defined principally by the degree of insufficiency produced by thermodynamic defects or chemical processes. Therefore, exergy analysis assists engineers in detecting the position and quantity of exergy destruction, allowing the application of process improvement measures.³⁶ The following expression gives the exergy equity of a control volume.

$$\dot{E} = \sum_i \left(1 - \frac{T_0}{T_i} \right) \dot{Q}_i - \dot{E}_{\text{work}} + \sum_i \dot{E}_{\text{in}} - \dot{E}_{\text{out}} - \dot{E}_{\text{D}} \quad (6)$$

where \dot{E} is the exergy rate; the temperatures of the surrounding and boundary air are T_0 and T_i , respectively; the heat flux across the control volume border is measured as \dot{Q}_i ; \dot{E}_{work} denotes the mechanical or electrical work; the exergy of the input and output streams is represented by \dot{E}_{in} and \dot{E}_{out} , respectively; and \dot{E}_{D} is the exergy destruction. It should be emphasized that \dot{E}_{in} and \dot{E}_{out} involve physical and chemical exergy.

2.4.1. Physical Exergy. Physical exergy refers to the maximum amount of thermodynamic work that can be generated by a state when it interacts with a reference state. Pressure potential energy is not considered because the pyrolysis occurs at atmospheric pressure. The enthalpy and entropy values required for calculating the physical exergy are derived through the Aspen Plus simulation. The physical exergy equations for gaseous $\text{ex}_{\text{ph-gas}}$ or solid–liquid $\text{ex}_{\text{ph-sol/liq}}$ are as follows.^{37,38}

$$\text{ex}_{\text{ph-gas}} = (h - h_0) - T_0(s - s_0) \quad (7)$$

$$\text{ex}_{\text{ph-sol/liq}} = c_p \left[(T - T_0) - T_0 \left(\ln \frac{T}{T_0} \right) \right] \quad (8)$$

h_0 and s_0 denote the enthalpy and entropy at a standard state temperature of 298 K and pressure of 1.01325 bar. The specific heat capacity c_p values of $\text{MgCl}_2 \cdot 6\text{H}_2\text{O}$ and $\text{MgCl}_2 \cdot \text{H}_2\text{O}$ are determined using the best-fitting curve supplied by Weck et al.;³⁹ the c_p of MgO is given as 1.22 kJ/kg·K.⁴⁰

2.4.2. Chemical Exergy. The chemical exergy of a material in a nonequilibrium environment is calculated to establish the standard exergy of a component. The chemical exergy of ideal gas mixtures is determined as follows³⁸

$$\text{ex}_{\text{ch-mix}} = \sum_i x_i \text{ex}_{\text{ch},i} + RT_0 \sum_i x_i \ln(x_i) \quad (9)$$

where x_i is the mole fraction of component i , R is the universal gas constant, and $e_{\text{ch},i}$ is the chemical exergy of component i . The chemical exergy of each component is calculated by eq 10, where n_j is the atomic number of element j in component i , $e_{\text{ch},j}$ is the chemical exergy of element j , and $\Delta G_{f,i}$ is the Gibbs free energy.

$$\text{ex}_{\text{ch},i} = \Delta G_{f,i} + \sum_j n_j \text{ex}_{\text{ch},j} \quad (10)$$

The chemical exergy of a gaseous fuel can be expressed as

$$\text{ex}_{\text{ch,fuel}} = \beta \times \text{LHV}_{\text{fuel}} \quad (11)$$

The factor β represents the ratio of the lower heating value (LHV) of the fuel to $e_{\text{ch,fuel}}$ chemistry exergy as a function of the C, H, and O atomic ratios.⁴¹ The LHV_{fuel} is determined by the molar proportion of each gas-phase component.

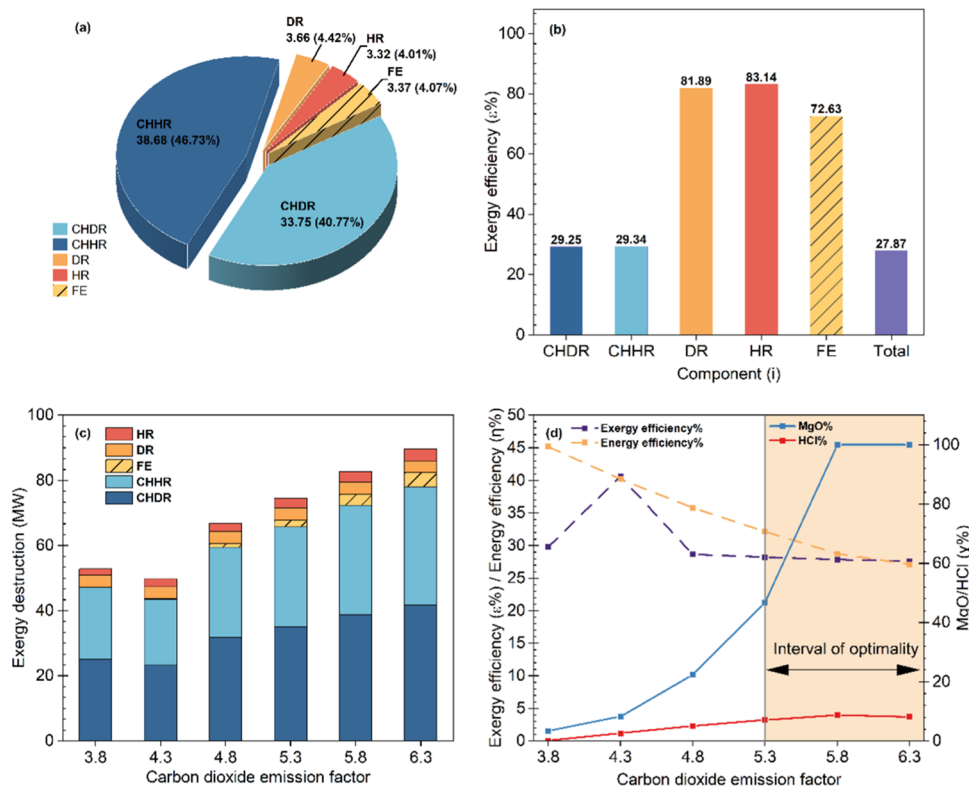


Figure 4. (a) Exergy destruction for each component in the bischofite pyrolysis pilot-scale system. (b) Exergy efficiency for each component in the bischofite pyrolysis process. (c) Effect of the carbon dioxide emission factor on exergy destruction. (d) Effect of the carbon dioxide emission factor on the production parameters.

$$\beta = \frac{1.0414 + 0.0177 \frac{H}{C} - 0.3328 \frac{O}{C} \left(1 + 0.0537 \frac{H}{C}\right)}{1 - 0.4021 \frac{O}{C}} \quad (12)$$

$$\text{LHV}_{\text{fuel}} = \sum_{i=1}^3 y_i \times \text{LHV}_i, \quad i = \text{CH}_4, \text{CO}, \text{C}_2\text{H}_6 \quad (13)$$

LHV_{fuel} denotes the lower heating value of the gas fuel (47.87 MJ/kg), and the factor β for the gas fuel is 1.10.

2.4.3. Performance Index. Considering the industrial applications, it is crucial to consider the system energy efficiency ($\eta\%$) and exergy efficiency ($\varepsilon\%$). Additionally, the yield of MgO ($\gamma\%$) is an important indicator of industrial production. The following equations can be used to determine these parameters

$$\eta = \frac{Q_{\text{py}} + Q_{\text{hc}} + Q_{\text{tr}}}{\beta \text{LHV}_{\text{fuel}}} \times 100\% \quad (14)$$

$$\varepsilon = 1 - \frac{E_{\text{D}}}{E_{\text{total}}} \times 100\% \quad (15)$$

$$\gamma = \frac{m_{\text{MgO}}}{m_{\text{solid}}} \times 100\% \quad (16)$$

Q_{py} is the heat required for the bischofite pyrolysis, Q_{hc} is the heat supplied to the heat consumer after flash, and Q_{tr} is the temperature rise for the MgO. E_{D} and E_{total} represent system exergy destruction and total input exergy, respectively. γ represents the MgO content in the solid product.

3. RESULTS AND DISCUSSION

3.1. Exergy Analysis of the System. In this section, we discuss the bischofite pyrolysis pilot-scale system exergy analysis. The goal of exergy analysis is to identify the component that causes the most exergy destruction. The process is complicated, involving heat transfer and complex chemical reactions of the material flow. We need to provide critical thermodynamic parameters such as standard chemical exergy and Gibbs energy to evaluate chemical exergy. Table S2 illustrates the standard chemical exergy derived for the process components. However, the physical exergy can be calculated from the enthalpy and entropy values obtained from the Aspen Plus software. Table S3 displays the thermodynamic parameters of the primary process streams.

The exergy destruction and efficiency for the bischofite pyrolysis are shown in Table S4 (Supporting Information). The pyrolysis process is separated into five components: flash evaporation (FE), dehydration reaction (DR), hydrolysis reaction (HR), combustion heating-dehydration reaction (CHDR), and combustion heating-hydrolysis reaction (CHHR). The bischofite pyrolysis system has an overall fuel exergy of 114.80 MW and a product exergy of 32.00 MW. The calculations reveal that overall the exergy destruction is 82.80 MW, leading to an exergy efficiency of 27.90%.

Notably, the larger destruction of the CHHR and CHDR units is mainly due to higher steam energy consumption and exothermic reactions. A large amount of water vapor produced during bischofite pyrolysis increases the exergy destruction of the combustion heating unit. Besides, the published literature has also established that exothermic processes and steam consumption heat significantly impact the extent of exergy

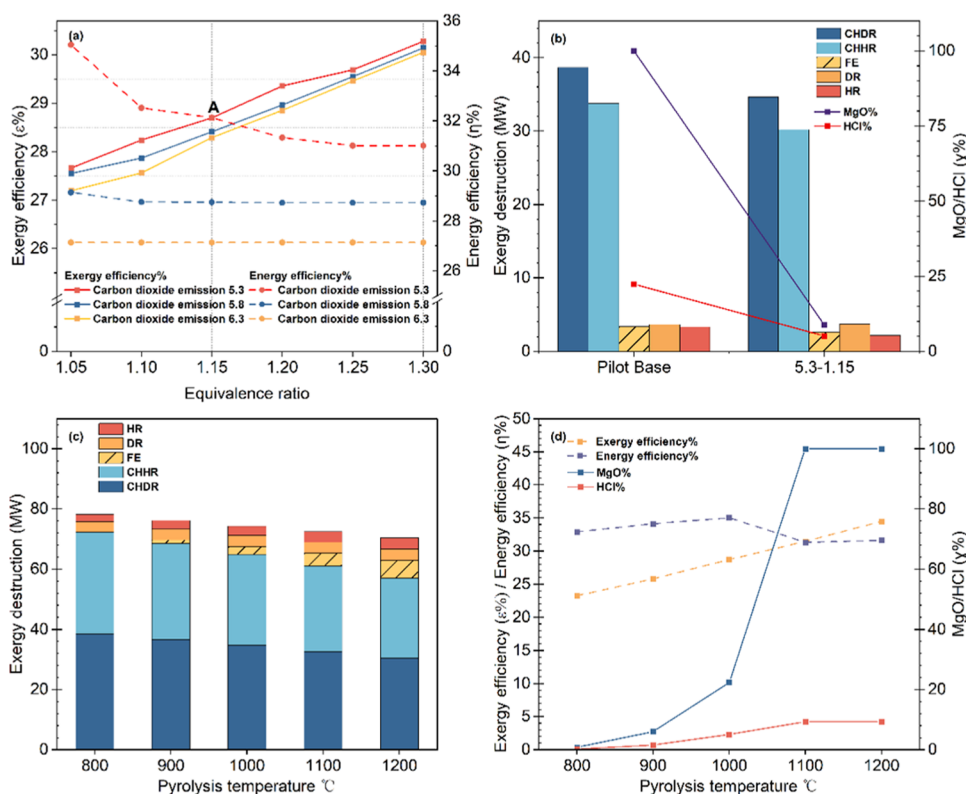


Figure 5. (a) Effect of carbon dioxide emission factor and equivalence ratio on exergy efficiency and energy efficiency. (b) Comparison of pilot conditions and the conditions with the carbon dioxide emission factor 5.3 and equivalence ratio 1.15. (c) Effect of pyrolysis temperature on exergy destruction at carbon dioxide emission factor 5.3 and equivalence ratio 1.15. (d) Effect of pyrolysis temperature on industrial parameters.

destruction in a system.²⁴ The other components are ranked in the following order, shown in Figure 4a: DR unit 3.66 MW (4.42%), FE unit 3.37 MW (4.07%), and HR unit 3.32 MW (4.01%). The DR and HR units have lower exergy destruction because dehydration and hydrolysis reactions are heat-absorbing. However, the enhanced physical and chemical exergy destruction of the decomposition products could be responsible for the residual exergy destruction.

Exergy efficiency is an important metric in exergy analysis used to evaluate the efficiency of the usable energy transfer in individual subunits. Figure 4b illustrates the exergy efficiency of each component in the pyrolysis system. The results show that in the CHDR and CHHR units, only 29.24 and 29.33% of the combustion heat is utilized for dehydration and hydrolysis, respectively. This indicates that a portion of the combustion heat is used for the pyrolysis reaction and heating of the product magnesium oxide, while the remainder is exergy destruction in the form of physical exergy. In contrast, the FE, HR, and DR units had relatively high exergy efficiency with low exergy destruction. Additionally, the overall system exergy efficiency of 27.87% is mainly influenced by the CHHR and CHDR units, which exhibit higher exergy destruction and lower exergy efficiency. As a result, retrofitting the CHHR and CHDR units presents a higher potential for improving the overall exergy efficiency relative to the other units.

A system exergy analysis revealed that the combustion heating unit is responsible for 86% of the total exergy destruction. Improving the combustion heating units can significantly enhance the overall exergy efficiency. The combustion stage is primarily impacted by the carbon dioxide emission factor, equivalent ratio, and pyrolysis temperature. This study

conducted parametric analysis (including carbon dioxide emission factor, equivalent ratio, and pyrolysis temperature) to estimate their effects on system exergy destruction and efficiency. In addition, the MgO yield, HCl concentration, and system energy efficiency were discussed to satisfy the production demands.

3.2. Effects of Carbon Dioxide Emission Factor. One of the prevalent parameters considered in bischofite pyrolysis is carbon dioxide emission factors, dividing the amount of carbon dioxide produced by the combustion of the gaseous fuel by the amount of bischofite converted to magnesium oxide (100%). The higher the carbon dioxide emission factors, the greater the fuel consumed, given a constant magnesium oxide production target. This ratio is generally considered in the range of 3.8–6.3 due to recent restrictions on carbon dioxide emissions from magnesium production.²¹ Figure 4c shows the effect of the carbon dioxide emission factor on the exergy destruction for each component. The other parameter settings are kept consistent with those of the pilot-scale system. The carbon dioxide emission factor of the pilot-scale system is 5.8. As demonstrated in Figure 4c, the overall exergy destruction increases as the carbon dioxide emission factor decreases and then increases. The reason for the increase in exergy destruction is that an increase in the fuel volume can lead to inadequate combustion and irreversible chemical exergy destruction when the air volume is constant. However, it is also necessary to investigate the effect of the carbon dioxide emission factor on MgO yield and HCl concentration, as shown in Figure 4d. Considering only exergy and energy efficiency, the carbon dioxide emission factor of 4.3 is the best option. However, a carbon dioxide emission factor of less than 5 causes only a 25%

MgO yield and less than 7% HCl concentration, the lowest amount at which hydrochloric acid can be produced industrially. Therefore, the carbon dioxide emission factor should be between 5.3 and 6.3 for optimal MgO yield and HCl concentration.

3.3. Effects of Equivalence Ratio. The equivalence ratio is a standard parameter in combustion processes, generally defined as the experimental air-to-fuel ratio to the stoichiometric air-to-fuel ratio, and is calculated using the following²⁶

$$ER = \frac{(\text{Air/Fuel})_{\text{exp}}}{(\text{Air/Fuel})_{\text{stoich}}} \quad (17)$$

The equivalence ratio is usually set at 1.05–1.3 to ensure complete fuel combustion. Figure 5a shows the influence of the carbon dioxide emission factor and equivalent ratio on the exergy efficiency and energy efficiency. The carbon dioxide emission factor ranges from 5.3 to 6.3, and the equivalent ratio ranges from 1.05 to 1.3. The results indicate that, for the same equivalent ratio, the smaller the carbon dioxide emission factor, the higher the exergy and energy efficiencies. For the same carbon dioxide emission factor, the exergy efficiency increases with the equivalent ratio, while the energy efficiency decreases. Therefore, the intersection point A is theoretically optimal when the carbon dioxide emission factor is 5.3 and the equivalent ratio is 1.15. Figure 5b compares pilot-scale conditions and the carbon dioxide emission factor of 5.3 to better illustrate the effect of each component's exergy destruction and industrial parameters. The increase in exergy efficiency is mainly attributed to the reduction in exergy destruction during combustion heating units (CHHR and CHDR units) and the decrease in chemical exergy destruction through complete combustion. The increase in exergy destruction in the HR and DR units is caused by a rise in flue gas temperature due to complete combustion. This increase in temperature affects the product's exergy in the pyrolysis and hydrolysis process, leading to an increase of physical exergy in these units. Industrially, the MgO yield was 22.35% with a HCl concentration of 5.09% at a carbon dioxide emission factor of 5.3 and an equivalence ratio of 1.15. This contrasts the pilot case, which produced 100% MgO yield and 8.77% HCl concentration. This is mainly attributed to the reduced fuel input, which provides less heat for the decomposition reaction and cannot fully satisfy the bischofite pyrolysis.

3.4. Effects of Pyrolysis Temperature. According to the parametric study of the carbon dioxide emission factor and equivalence ratio, the carbon dioxide emission factor is 5.3, and the equivalence ratio is 1.15, higher than the exergy and energy efficiency under the pilot-scale conditions. Unfortunately, the current industrial production data are insufficient to meet production requirements. To tackle this challenge, it is crucial to examine the impact of various parameters within the pyrolysis furnace on the exergy, energy efficiency, and industrial parameters. Among these parameters, the pyrolysis temperature significantly affects the MgO yield, HCl concentration, and the quality of MgO. Industrial data and research suggest that pyrolysis temperatures range from 800 to 1200 °C.⁴² The aforementioned parameters, carbon dioxide emission factor, and equivalence ratio were tested at a pyrolysis temperature of 1000 °C. Further investigation is required to determine the impact on exergy destruction, system energy efficiency, and industrial parameters at a carbon dioxide emission factor of 5.3, an equivalence ratio of 1.15, and decomposition temperatures

between 800 and 1200 °C, as illustrated in Figure 5c. The results show that exergy destruction gradually decreases as the pyrolysis temperature rises. This is primarily due to a decrease in the exergy destruction caused by an increase in the thermal efficiency of the combustion process. However, the exergy destruction of FE, DR, and HR tends to increase. These are caused by the high pyrolysis environment, which enhances the physical exergy of the exit flue gases and byproducts by raising the temperature of decomposition products. Based on the industrial production data analysis, it has been revealed that a decomposition temperature above 1000 °C leads to better results, as shown in Figure 5d. The main performance is that the conversion rate of magnesium oxide is 100%, and the concentration of hydrogen chloride is above 9.33%. Above 1000 °C, the energy efficiency decreases with increasing temperature, while exergy efficiency increases with increasing temperature. Thus, 1100 °C is the preferred temperature. Compared to 1000 °C, the energy efficiency decreased by 3.73%, the exergy efficiency increased by 2.79%, the yield of MgO increased by 77.6%, and the concentration of HCl increased by 4.24%. In addition, the energy efficiency was increased by 3.66%, and the utilization efficiency was increased by 2.51% compared with the pilot conditions.

4. CONCLUSIONS

In this work, the pilot-scale pyrolysis process from bischofite industrial waste was simulated by using Aspen Plus software, and exergy analysis was conducted to quantify the exergy destruction in the process. Given the complexity of the bischofite decomposition process, a continuous modular modeling approach was used to simulate the dehydration and hydrolysis reactions in a pyrolysis furnace. These reactions were implemented by integrating a FORTRAN subroutine within Aspen Plus. In addition, the exergy efficiency and energy efficiency were optimized regarding the carbon dioxide emission factor, equivalence ratio, and pyrolysis temperature. The conclusions are as follows.

1. Under pilot-scale conditions, the bischofite pyrolysis system has an exergy efficiency of 27.9% and exergy destruction of 82.8 MW. CHHR and CHDR units contribute significantly to exergy destruction, accounting for 46.73 and 40.77%, respectively. This indicates that the combustion phase is the main bottleneck in terms of energy consumption.
2. With the increase of the carbon dioxide emission factor, the system exergy destruction shows a trend of first decreasing and then increasing. The increase in system exergy destruction is mainly due to the rise in irreversible chemical exergy caused by inadequate combustion. As a result, the carbon dioxide emission factor of 4.3 is considered adequate, but the MgO yield and HCl concentration will not fulfill the objectives of industrial production. It is advised that the carbon dioxide emission factor be between 5.3 and 6.3 to match the actual production conditions.
3. For carbon dioxide emission factors between 5.3 and 6.3, the effect of equivalence ratios on energy efficiency and exergy efficiency was investigated. The smaller the emission factor, the higher the energy and exergy efficiencies. Increasing the equivalent ratio under the same emission factor can improve exergy efficiency but reduce energy efficiency. The optimal energy and exergy

efficiency values occur at a carbon dioxide emission factor of 5.3 and an equivalence ratio of 1.15. Nevertheless, heat absence causes bischofite to decompose incompletely, with the MgO yielding only 22.35% and a HCl concentration of 5.09%.

- When the carbon dioxide emission factor is 5.3, and the equivalence ratio is 1.15, the overall exergy destruction is steadily reduced as the pyrolysis temperature increases. Because of increased combustion process thermal efficiency, there was less exergy destruction. Based on the MgO yield and HCl concentration, 1100 °C is the ideal temperature for pyrolysis.
- The optimal pilot-scale conditions consist of a carbon dioxide emission factor of 5.3, an equivalence ratio of 1.15, and a pyrolysis temperature of 1100 °C. Under the optimal conditions, energy efficiency is notably improved by 3.66% and exergy efficiency by 2.51%. Additionally, the carbon dioxide emission factor decreases from 5.8 to 5.3. Furthermore, the process yields 100% MgO production and a HCl concentration exceeding 9.33%. Overall, the study demonstrated the potential for converting bischofite waste into valuable MgO through pilot-scale experiments and thermodynamic analyses, which could guide future commercialization and scale-up.

■ ASSOCIATED CONTENT

SI Supporting Information

The Supporting Information is available free of charge at <https://pubs.acs.org/doi/10.1021/acsomega.3c07165>.

Operating conditions of the bischofite pyrolysis pilot-scale process (Table S1); standard chemical exergy (Table S2); thermodynamic details or parameters of the main process streams (Table S3); and exergy destruction and efficiency calculation in each component of the bischofite pyrolysis system (Table S4) (PDF)

■ AUTHOR INFORMATION

Corresponding Author

Hui Dong – SEP Key Laboratory of Eco-industry, School of Metallurgy, Northeastern University, Liaoning, Shenyang 110819, China; orcid.org/0009-0005-4222-2183; Email: Helenxululu@outlook.com

Authors

Hanlu Xu – SEP Key Laboratory of Eco-industry, School of Metallurgy, Northeastern University, Liaoning, Shenyang 110819, China

Liang Zhao – SEP Key Laboratory of Eco-industry, School of Metallurgy, Northeastern University, Liaoning, Shenyang 110819, China

Daokuan Cheng – SEP Key Laboratory of Eco-industry, School of Metallurgy, Northeastern University, Liaoning, Shenyang 110819, China

Complete contact information is available at:

<https://pubs.acs.org/doi/10.1021/acsomega.3c07165>

Author Contributions

[†]H.X. and D.C. contributed equally to this work.

Notes

The authors declare no competing financial interest.

■ ACKNOWLEDGMENTS

This project was generously funded by the Jiebangguashuai Foundation of Liaoning Province, China (2021JH1/10400030) and the National Key R&D Program of China's Technologies and Integrated Application of Magnesite Waste Utilization for High-Valued Chemicals and Materials' (2020YFC1909303).

■ NOMENCLATURE

Y_{mass} fraction (%)
 \dot{E} exergy rate (W)
 T temperature (K)
 \dot{Q} heat flux (W)
 e_{specific} specific exergy (kJ/kg)
 h_{specific} specific enthalpy (kJ/kg)
 s_{specific} specific entropy (kJ/kg·K)
 c_p specific heat capacity (kJ/kg·K)
 ΔG_f Gibbs energy of chemical formation (kJ/mol)
 n atomic number (–)
 m mass (kg)

■ GREEK SYMBOLS

β ratio of the lower heating value (–)
 η energy efficiency (%)
 ϵ exergy efficiency (%)
 γ MgO content (%)

■ SUBSCRIPTS

o operation data
 s simulation data
 w mechanical or electrical work
 i input streams
 o output streams
 D destruction
 i component i
 O standard state
 p physical
 g gaseous
 sol/liq solid or liquid
 ch chemical
 j element j
 f fuel gaseous fuel
 py bischofite pyrolysis
 h heat consumer
 tr temperature rise

■ ABBREVIATIONS

FE flash evaporation
 DE dehydration reaction
 HR hydrolysis reaction
 CHDR combustion heating-dehydration reaction
 CHHR combustion heating-hydrolysis reaction
 TG thermogravimetric analysis
 LHV lower heating value

■ REFERENCES

- An, J.; Li, Y.; Middleton, R. S. Reducing energy consumption and carbon emissions of magnesite refractory products: A life-cycle perspective. *J. Cleaner Prod.* **2018**, *182*, 363–371.
- Ren, W.; Xue, B.; Lu, C.; Zhang, Z.; Zhang, Y.; Jiang, L. Evaluation of GHG emissions from the production of magnesite refractory raw materials in Dashiqiao, China. *J. Cleaner Prod.* **2016**, *135*, 214–222.

- (3) U.S. Geological Survey Releases 2022 List Critical Minerals; United States Geological Survey: 2022.
- (4) Guo, T.; Geng, Y.; Song, X.; Rui, X.; Ge, Z. Tracing magnesium flows in China: A dynamic material flow analysis. *Resour. Policy* **2023**, *83*, No. 103627.
- (5) Huang, Q.; Zheng, W.; Dong, J.; Wen, J.; Chang, C.; Xiao, X. Influences of different bischofite on the properties of magnesium oxychloride cement. *J. Build. Eng.* **2022**, *57*, No. 104923.
- (6) Gutierrez, A.; Ushak, S.; Galleguillos, H.; Fernandez, A.; Cabeza, L. F.; Grágeda, M. Use of polyethylene glycol for the improvement of the cycling stability of bischofite as thermal energy storage material. *Appl. Energy* **2015**, *154*, 616–621.
- (7) Wu, J.; Sun, Q.; Lu, J. Synthesis of magnetic core-shell FeO@SiO₂@Mg(OH) composite using waste bischofite and its catalytic performance for ozonation of antibiotics. *J. Environ. Chem. Eng.* **2020**, *8* (5), No. 104318.
- (8) Li, P.; Liu, B.; Lai, X.; Liu, W.; Gao, L.; Tang, Z. Thermal decomposition mechanism and pyrolysis products of waste bischofite calcined at high temperature. *Thermochim. Acta* **2022**, *710*, No. 179164.
- (9) Yang, Q.; Gao, X.; Fang, L.; Zhang, S.; Cheng, F. Controllable crystal growth of Mg(OH)₂ hexagonal flakes and their surface modification using graft polymerization. *Adv. Powder Technol.* **2021**, *32* (7), 2634–2644.
- (10) Statistics Bureau of Qinghai Province. *Qinghai Province Statistical Bulletin of National Economic and Social Development in 2019* Statistics Bureau of Qinghai Province: China; 2019.
- (11) Lin, S.; Zhang, T.; Fu, D.; Zhou, X. Utilization of magnesium resources in salt lake brine and catalytic degradation of dye wastewater by doping cobalt and nickel. *Sep. Purif. Technol.* **2021**, *270*, No. 118808.
- (12) Liu, W.; Xu, H.; Cheng, J.; Li, G.; Yang, X. Effects of base liquid on the settlement property of Mg(OH)₂ prepared by the lime method. *Mater. Rev.* **2012**, *26*, 313–316.
- (13) Liu, W.; Xu, H.; Shi, X.; Yang, X.; Wang, X. Improved lime method to prepare high-purity magnesium hydroxide and light magnesia from bischofite. *JOM* **2019**, *71*, 4674–4680.
- (14) Xu, H.; Cai, Y.; Shi, X.; Pi, G. H. Study on preparation of high purity magnesia from brucite. *J. Nat. Sci. Hunan Normal Univ.* **2006**, *29*, 52–55.
- (15) Mizrahi, J. *Developing an Industrial Chemical Process: an Integrated Approach*, 1st ed.; CRC Press LLC, 2002.
- (16) Epstein, J. A. Utilization of the dead sea minerals (a review). *Hydrometallurgy* **1976**, *2* (1), 1–10, DOI: 10.1016/0304-386X(76)90009-8.
- (17) Seeger, M.; Otto, W.; Flick, W.; Bickelhaupt, F.; Akkerman, O. S. Magnesium Compounds. *Ullmann's Encycl. Ind. Chem.* **2011**, *2*, 41–77.
- (18) Zhang, H.; Cao, T.; Cheng, Y. Synthesis of nanostructured MgO powders with photoluminescence by plasma-intensified pyrohydrolysis process of bischofite from brine. *Green. Process. Synth.* **2014**, *3* (3), 215–222, DOI: 10.1515/gps-2014-0026.
- (19) Yager, T. R.; National Minerals Information Center. The Mineral Industry of Israel, 2016. <https://www.usgs.gov/media/files/mineral-industry-israel-2016-pdf> (accessed October 02, 2016).
- (20) Du, W.; Sun, Z.; Lu, G.; Yu, J. Interaction between a hollow-cone spray and the co-axial swirling stratified flow in a novel spray pyrolysis furnace. *Can. J. Chem. Eng.* **2018**, *96*, 1079–1088.
- (21) Bakker, J. D. The recovery of magnesium oxide and hydrogen chloride from magnesium chloride brines and molten salt hydrates. Ph.D. Dissertation Queen's University: Kingston, Ontario, Canada, 2011.
- (22) Luong, V. T.; Amal, R.; Scott, J. A.; Ehrenberger, S.; Tran, T. A comparison of carbon footprints of magnesium oxide and magnesium hydroxide produced from conventional processes. *J. Cleaner Prod.* **2018**, *202*, 1035–1044.
- (23) Gollangi, R.; NagamalleswaraRao, K. Energy, exergy analysis of conceptually designed monochloromethane production process from hydrochlorination of methanol. *Energy* **2022**, *239*, No. 121858.
- (24) Mohamadi-Bagholaei, M.; Hajizadeh, A.; Zendeheboudi, S.; Duan, X.; Shiri, H. Advanced Exergy Analysis of an Acid Gas Removal Plant to Explore Operation Improvement Potential toward Cleaner Production. *Energy Fuels* **2021**, *35* (11), 9570–9588.
- (25) Arteaga-Díaz, S. J.; Meramo, S.; González-Delgado, A. D. Computer-aided modeling, simulation, and exergy analysis of large-scale production of magnetite (Fe₃O₄) nanoparticles via coprecipitation. *ACS Omega* **2021**, *6* (45), 30666–30673.
- (26) HajiHashemi, M.; Mazhko, S. M.; Dadfar, H.; Livani, E.; Varnosefaderani, A. N.; Pourali, O.; Nobar, S. N.; Dutta, A. Combined heat and power production in a pilot-scale biomass gasification system: Experimental study and kinetic simulation using Aspen Plus. *Energy* **2023**, *276*, No. 127506.
- (27) Chen, X.; Jin, X.; Ling, X.; Wang, Y. Exergy analysis of concentrated solar power plants with thermochemical energy storage based on calcium looping. *ACS Sustainable Chem. Eng.* **2020**, *8* (21), 7928–7941.
- (28) Liu, X.; Yu, M.; Liu, Z.; Yang, S. Exergy analysis and advanced exergy analysis of a novel power/refrigeration cascade system for recovering low-grade waste heat at 90–150 °C. *ACS Sustainable Chem. Eng.* **2022**, *10* (28), 9184–9193.
- (29) Xu, H.; Dong, H.; Zhao, L.; Zhang, M.; Cheng, D. Isoconversional kinetic analysis of the pyrolysis of Salt Lake industrial waste bischofite with isothermal reaction time predictions. *Process. Saf. Environ. Prot.* **2023**, *169*, 725–735.
- (30) Park, J.; Kim, Y.; Lim, J.; Cho, H.; Kim, J. Optimal operation of the evaporator and combustion air distribution system in a pulp mill to maximize biomass recycling and energy efficiency. *J. Cleaner Prod.* **2022**, *367*, No. 133048.
- (31) Huang, Q.; Lu, G.; Wang, J.; Yu, J. Thermal decomposition mechanisms of MgCl₂·6H₂O and MgCl₂·H₂O. *J. Anal. Appl. Pyrolysis* **2011**, *91*, 159–164.
- (32) Yu, J.; Sun, L.; Ma, C.; Qiao, Y.; Xiang, J.; Hu, S.; Yao, H. Mechanism on heavy metals vaporization from municipal solid waste fly ash by MgCl₂·6H₂O. *Waste Manage.* **2016**, *49*, 124–130.
- (33) Sugimoto, K.; Dinneber, R. E.; Hanson, J. C. Structures of three dehydration products of bischofite from in situ synchrotron powder diffraction data (MgCl₂·nH₂O; n = 1, 2, 4). *Acta Crystallogr., Sect. B: Struct. Sci.* **2007**, *63* (2), 235–242.
- (34) Trninić, M.; Stojiljković, D.; Manić, N.; Skreibeberg, Ø.; Wang, L.; Jovović, A. A mathematical model of biomass downdraft gasification with an integrated pyrolysis model. *Fuel* **2020**, *256*, No. 116867.
- (35) Mohamadi-Bagholaei, M.; Hajizadeh, A.; Zahedizadeh, P.; Azin, R.; Zendeheboudi, S. Evaluation of hybridized performance of amine scrubbing plant based on exergy, energy, environmental, and economic prospects: A gas sweetening plant case study. *Energy* **2021**, *214*, No. 118715.
- (36) Szargut, J.; Morris, D. R.; Steward, F. R. *Exergy Analysis of Thermal, Chemical, and Metallurgical Processes*, 1st ed.; Hemisphere, 1987.
- (37) Meramo-Hurtado, S. I.; González-Delgado, A.; Rehmman, L.; Quinones-Bolanos, E.; Mehvar, M. Comparative analysis of biorefinery designs based on acetone-butanol-ethanol fermentation under exergetic, techno-economic, and sensitivity analyses towards a sustainability perspective. *J. Cleaner Prod.* **2021**, *298*, No. 126761.
- (38) Fan, C.; Cui, Z.; Wang, J.; Liu, Z.; Tian, W. Exergy analysis and dynamic control of chemical looping combustion for power generation system. *Energy Convers. Manage.* **2021**, *228*, No. 113728.
- (39) Weck, P. F.; Kim, E. Solar energy storage in phase change materials: first-principles thermodynamic modeling of magnesium chloride hydrates. *J. Phys. Chem. C* **2014**, *118*, 4618–4625.
- (40) Yaws, C. L. *Chemical Properties Handbook: Physical, Thermodynamics, Environmental Transport, Safety & Health Related Properties for Organic & Inorganic Chemicals*; McGraw Hill Handbooks, 1999.
- (41) Arslan, M.; Yilmaz, C. Thermodynamic optimization and thermoeconomic evaluation of afyon biogas plant assisted by organic rankine cycle for waste heat recovery. *Energy* **2022**, *248*, No. 123487.
- (42) Aman, J. J. Improvements in or relating to the thermal decomposition of certain chlorides and sulphates. IE22729B1, 1954.